applied optics

996 nm high-power single-longitudinal-mode tapered gain-coupled distributed feedback laser diodes

Yuxin Lei,[1,2] Yongyi Chen,[1,*] Feng Gao,[1,3] Dezheng Ma,[1,2] Peng Jia,[1,4] Hao Wu,[1] Chunkao Ruan,[1,2] Lei Liang,[1] Chao Chen,[1] Jun Zhang,[1] Li Qin,[1] Yongqiang Ning,[1] and Lijun Wang[1]

[1]State Key Laboratory of Luminescence and Application, Changchun Institute of Optics, Fine Mechanics and Physics, Chinese Academy of Sciences, Changchun 130033, China
[2]University of Chinese Academy of Sciences, Beijing 100049, China
[3]e-mail: summit1990@163.com
[4]e-mail: jiapeng@ciomp.ac.cn
*Corresponding author: chenyy@ciomp.ac.cn

Received 27 December 2018; revised 28 February 2019; accepted 8 April 2019; posted 8 April 2019 (Doc. ID 356135); published 9 August 2019

A high-power single-longitudinal-mode regrowth-free tapered gain-coupled distributed feedback laser diode based on periodic current injection is achieved at 996 nm. It enhances the output power without beam quality degrading. A continuous-wave output power of over 1.12 W is achieved at 3 A. The maximum output power in single-longitudinal-mode operation is up to 0.56 W at 1.4 A. The power conversion efficiency is over 24%, and the slope efficiency is 0.58 W/A. The side mode suppression ratio is over 38 dB; the 3 dB spectral linewidth is less than 2.4 pm. The lateral far-field divergence angle is only 14.98°, and the beam quality factor M^2 is 1.64, achieving a near-diffraction-limit emission. Our device has great potential in commercial applications and the experimental study of high-power near-diffraction-limit laser diodes for its low-cost fabrication technique and narrowband single-longitudinal-mode emission at high power.

https://doi.org/10.1364/AO.58.006426

1. INTRODUCTION

Distributed feedback (DFB) semiconductor lasers are extensively used in multitude application fields, such as high-efficiency pumping sources [1], medicine and biology [2], telecommunications [3,4], material processing [5], gas sensing [6], lidar [7–9], and integrated optics [10] as a reliable source. It is expected to achieve high power, high beam quality, and narrow linewidth in stable single-longitudinal-mode (SLM) operation with a low-cost and easy fabrication technique [11,12]. On the one hand, traditional index-coupled [13] and gain-coupled DFB [14,15] lasers with mode-selection gratings are widely used to achieve SLM operation by filtering unwanted longitudinal modes, but they usually have low output powers [16], and both of them suffer from unavoidable problems, as discussed in Ref. [17]. Solutions to these problems such as phase shift gratings [18,19], reconstruction equivalent-chirp (REC) [20,21] and other methods usually require complicated, precise, and high-cost fabrication techniques. The fabrication technique makes them difficult to maintain consistency in volume production. On the other hand, high-power lasers often suffer from multitude-longitudinal-mode (MLM) operation and heat accumulation [22]. The MLM operation tends to produce mode competition, which leads to the degradation of side-mode suppression ratio (SMSR) or even mode hopping [23]. The tapered structure [24–26] is commonly introduced to enhance the output power while maintaining the high beam quality. But the tapered laser usually suffers from spatial hole burning (SHB) at high output power [22]. Separated electrode contacts, which require complex fabrication and package steps, are proposed to get over the problem, while causing the instability from the precise control of the currents and temperatures for different segments [27].

In this paper, we propose a high-power regrowth-free tapered gain-coupled DFB laser with periodic p-electrodes to achieve high output power in SLM operation with high SMSR and narrow linewidth. The maser oscillator power amplifier (MOPA) structure, which consists of a ridge waveguide and a tapered waveguide, is used to amplify the output power in SLM operation and high beam quality. The high-order surface gain-coupled gratings insulated by periodic shallow-etched grooves filled with silica lead to periodic injection current [14]. The gain-coupled mechanism is formed by gain contrast in quantum wells without introducing an effective index-coupled effect. The improved fabrication process of our tapered gain-coupled DFB laser requires only ordinary i-line lithography and dry etching without expensive, complicated, and

time-consuming processing steps such as nanometer-scale lithography [28,29], second epitaxy growth [20], or high-quality antireflection facet coating techniques [14]. With such a simple and low-cost technique, our device still provides excellent performance. The continuous-wave (CW) output power is up to 1.12 W at 3 A with a slope efficiency of over 0.58 W/A. The maximum electro-optical efficiency is over 24.5%. SLM emitting is achieved from the threshold to 1.4 A. The enhanced maximum CW output power in SLM operation is more than 0.56 W, which is an order of magnitude higher than our previously reported SLM lasers [17,30]. The narrow 3 dB spectral linewidth is less than 2.4 pm. The high SMSR of 38 dB is achieved at 996 nm. The lateral far-field divergence angle is 14.98°, and the beam quality factor M^2 is 1.64, achieving a near-diffraction-limit emission. Our tapered gain-coupled DFB laser device provides a low-cost method to fabricate high-power high-beam-quality SLM lasers for widespread practical applications, and it would receive great attention due to the simplified fabrication process, easy fabrication technique, and excellent performance.

2. DEVICE DESIGN AND FABRICATION

Figure 1 shows the schematic diagram of our tapered gain-coupled DFB laser device. As shown in Fig. 1(a), our 2-mm-long, 0.5-mm-wide device consists of an 800-μm-long, 6-μm-wide ridge waveguide and a 1200-μm-long tapered waveguide with a full tapered angle less than 4°; the corresponding width of the output facet is 100 μm. A self-designed ultralow aluminum asymmetric ultralarge optical-cavity (ULOC) wide waveguide separate confinement heterostructure (SCH) with a compressively strained InGaAs quantum wells wafer [31] is used to reach high power and a small vertical far-field divergence angle. As shown in Fig. 1(b), the p-confinement layer consists of a 0.5 μm low-index cladding layer and a 1.2 μm high-index waveguide layer. The combination of the ridge waveguide and the tapered waveguide forms a MOPA structure that is used to enhance the output power in SLM operation and fundamental-transverse-mode (FTM) operation. Detailed parameters of the ridge waveguide and tapered waveguide are meticulously designed in consideration of theory and experimental conditions to obtain high power and high beam quality.

The ridge waveguide in our device plays a key role and serves as a modal filter to provide FTM and SLM operation. Leaving the unetched ridge sandwiched between the etched slabs aside, it is equivalent to be treated as solving fundamental modes as the three-layer slab waveguide [32]. The width of the ridge waveguide is expected to be wider to increase the output power, process tolerance, and catastrophic optical damage (COD) threshold of the rear facet and is finally set to be 6 μm to achieve FTM operation and low threshold current as well. The etching depth is determined in consideration of the balance between the effective optical field restriction and the minimum optical field loss. The corresponding light field pattern is calculated by the commercial software COMSOL Multiphysics. The single-mode operation is achieved with the ridge waveguide width of 6 μm and the etching depth of 1.3 μm; the FTM optical field distribution is shown in Fig. 2.

The SLM narrowband emission is beneficial from the additional wavelength selective feedback supplied by the gain-coupled DFB structure in the ridge waveguide. The gain contrast in quantum wells of the gain-coupled DFB laser is achieved by the periodic current injection from periodic surface metal p-contacts and periodic shallow-etched surface grooves insulated by silica, as the schematic diagram depicts in Fig. 1(e). As demonstrated in Ref. [17], the insulated shallow-etched grooves can effectively increase the gain contrast in the quantum wells. The coupling coefficient κ demonstrates the strength of the gain coupling mechanism; the coupling coefficient κ of our gain-coupled DFB device is $\kappa = i\frac{\Delta g\Gamma}{4}$, where Δg is the gain/loss contrast in the waveguide, and Γ is the optical confinement factor in the quantum wells. As can be seen, κ is independent of the grating period; we use

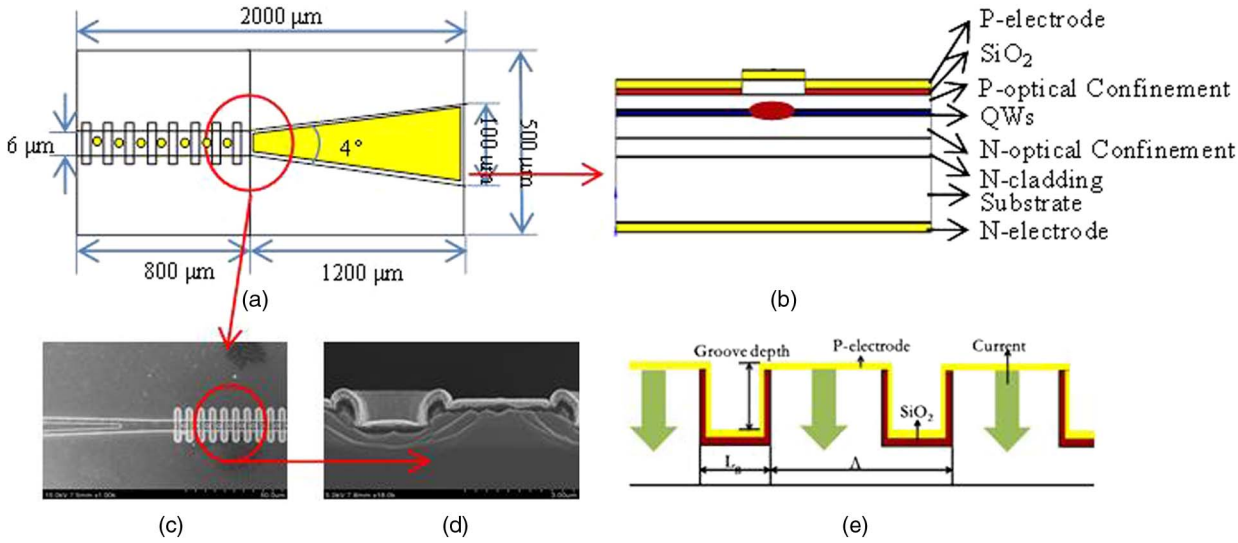

Fig. 1. Schematic diagram of the tapered gain-coupled DFB laser device. (a) Layout of the tapered gain-coupled DFB laser with periodic electrodes; (b) epitaxial layer structure; (c) SEM image of the periodic surface electrodes from top view; (d) SEM image of the periodic surface-etched grooves from lateral view; (e) periodic current injection schematic.

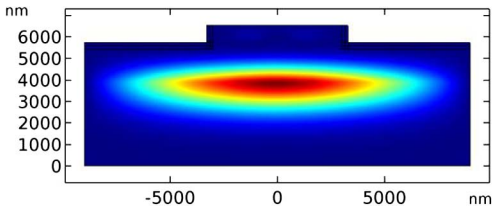

Fig. 2. Optical field distribution of the gain-coupled DFB laser device with a ridge width of 6 μm and an etching depth of 1.3 μm.

micrometer-scale high-order insulated surface grooves to achieve a gain-coupled mechanism and reduce processing difficulty. As the scanning electron microscope (SEM) image shows in Fig. 1(d), the surface grooves are modeled as a rectangular shape with a length of 2 μm. The micrometer-scale grooves are not as precise as nanometer-scale grating [29], apodized grating [28], or deeply etched gratings with high diffraction efficiencies; hence it only requires i-line lithography and ordinary ion etching with high reproducibility. Besides, in comparison with electron-beam lithography, i-line lithography is more practical and applicable in actual production for realizing structures with low costs and simplified manufacturing processes. The periodic electrodes and the periodic shallow-etched grooves share the same large period of 6.12 μm. Then, the periodic shallow-etched grooves periodically modulate the optical field and achieve an SLM narrowband emission. The depth of the grooves depends on the residual layer's thickness, which is the distance between the bottom of the surface grooves and the top of the quantum wells. The residual layer's thickness should be thin enough to restrict the distribution of carriers for high gain contrast in quantum wells, and thick enough to avoid introducing an effective index-coupled effect for less optical scattering loss [14]. The depth of the shallow-etched grooves has been exactly designed and finally determined as 0.7 μm, according to the optical field distribution calculated by BeamProp software; this is shown in Fig. 3. As the SEM image shows in Fig. 1(c), the grooves are 20 μm wide, which is much wider than the ridge width. The excess parts aside the ridge waveguide are used to act as isolation-leaking grooves. They can filter out high-order transverse modes to help maintain FTM, and filter out backreflection from the tapered waveguide to suppress the nonlinear effect, such as SHB and the filament

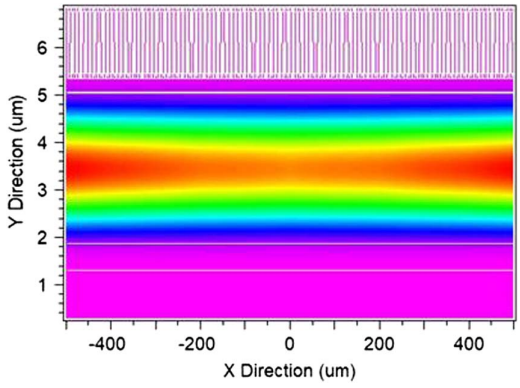

Fig. 3. Optical field distribution profile of gain-coupled DFB laser device.

effect, which would cause the deterioration of the modal filtering efficiency [33]. The isolation-leaking grooves are formed in the same simple process with the gain-coupled grating without additional steps, as most leaking grooves in published tapered lasers require [33]. Thus, the SLM operation is achieved with a simple fabrication technique.

The tapered waveguide is used for optical amplification to enhance the output power in SLM and FTM operation. The full tapered angle of the tapered waveguide is obtained by referring to the fundamental mode diffraction angle at $1/e^2$ [34] and is finally defined to be 4°. The proper tapered angle prevents high-order modes coupling into the fundamental mode and increases the high-order mode loss during transmission. The lengths of the ridge waveguide and tapered waveguide derive from the balance of the mode filtering and power amplification. A longer ridge waveguide would provide much more effective mode filtering, and a longer tapered waveguide would provide a larger current injection area, resulting in greater power amplification. The length of the tapered waveguide further relates to the surface area of the output facet, which determines the width of the aperture as the transverse field profile at a different position along the z axis calculated by BeamProp software; this is shown in Fig. 4. The tapered waveguide length of 1200 μm is chosen to fully amplify the power; the calculated power-current-voltage (PIV) curves are shown in Fig. 5. The gradually varied width from 6 to 100 μm provides more scattering loss for high-order transverse modes than FTM when the modes are expanded and shrunken in the waveguides [29]. As shown in Fig. 4, the FTM operation could be obtained at any cross sections along the direction of the cavity. And the power density is significantly reduced by remarkably increasing the emitting aperture; then the threshold of COD at output facet is dramatically improved. The width of the tapered waveguide is gradually expanded to reduce the optical power density of the light propagation field; then the nonlinear effects such as SHB or the filament effect caused by self-focusing effect are effectively avoided. The index-guided mechanism of the tapered waveguide is used for more effective restriction of light distribution rather than the gain-guided mechanism; thus, the slow-axis far-field divergence angle of our device is dramatically reduced. Thanks to the fact that the index-guided tapered waveguide can be formed simultaneously with the ridge waveguide, the fabrication process is simplified as well. Hence, our tapered waveguide achieves the power amplification and maintains the excellent beam quality without additional fabrication steps.

The epitaxial layer structure described in Ref. [31] was grown by metal organic chemical vapor deposition (MOCVD) based on a GaAs substrate. After the material growth, the grooves, the mesa, and the electrodes were precisely defined and formed by standard i-line lithography and inductively coupled plasma (ICP) dry etching techniques in sequence. A silica layer was deposited on the wafer by plasma-enhanced chemical vapor deposition (PECVD) to become hard masked. The periodic shallow-etched grooves in the ridge waveguide with a period around 6.12 μm were formed by etching through the p-side of the wafer to the vertical structure into the waveguide layer. The lateral waveguide of the MOPA structure was

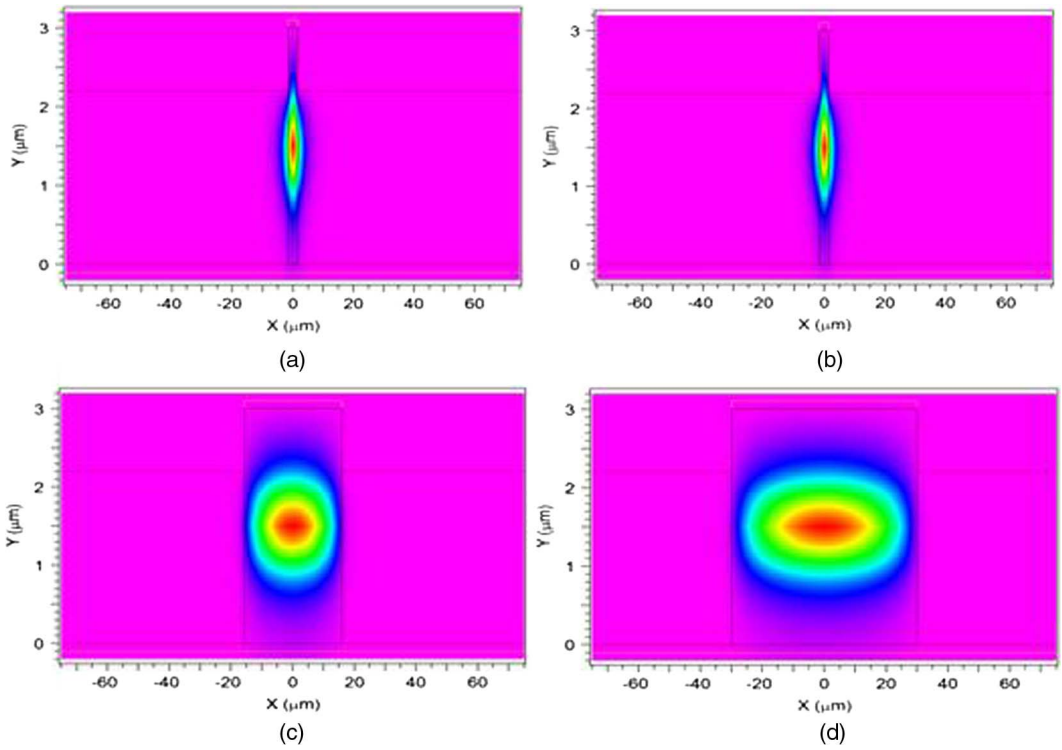

Fig. 4. Transverse field profile of the tapered waveguide at different positions along the z axis. (a) $z = 0$; (b) $z = 800$; (c) $z = 1100$; (d) $z = 1500$.

practically etched to 1.3 μm to achieve FTM operation by restricting other high-order modes. Before the formation of the periodic current injection windows, a silica layer was deposited again to become hard masked in the etching, electrical insulation, and loss absorption of optical field from the top contact of the grooves. Periodic surface metal p-electrodes were formed after electroplating gold and metallization. A metal n-electrode was formed by electroplating gold and metallization after lapping with 150 μm. Then, the wafer was cleaved into bars with a cavity length of 2 mm. The laser bars were then cleaved into 500-μm-wide single emitters after coating with antireflectivity (AR)/high-reflectivity (HR) films on the front/rear facets, respectively. Single emitters were mounted p-side down on AlN sub-mounts with hard solder. Golden wire bonding was used to contact the n-side with the sub-mounts for CW measurement. Then, the chips on the sub-mounts were mounted on copper heat sinks for water-cooling in further testing and analysis.

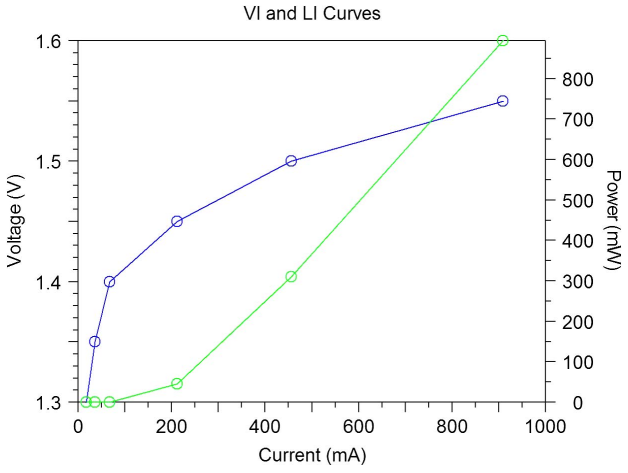

Fig. 5. Calculated PIV curves of the tapered laser.

3. RESULTS AND DISCUSSION

Device testing was performed under CW conditions at a heat-sink temperature of 20°C. All measurement devices for comparisons were fabricated simultaneously from the same wafer. The optical output power was measured with a national-standard thermoelectric detector directly placed in front of the output facet. Current and voltage were measured directly with the power supply. The optical spectrum was measured with a 10 μm core diameter fiber-linking YOKOGAWA AQ6370C optical spectrum analyzer. It was checked that the measured spectra, especially the peak positions, were not affected by the position of the fiber, and the results were reproducible. The linewidth was measured by coupling the collimating laser into a Fabry–Perot (FP) interferometer (Thorlabs, SA200-8B). The resolution of the FP interferometer is 67 MHz, and the free spectral range of the FP interferometer is 10 GHz. The beam waist width was measured after collimation with a fast-axis collimating lens, a slow-axis collimating lens, and a focusing lens.

The PIV characteristics and electro-optical efficiency profiles of the coated tapered gain-coupled DFB laser device under

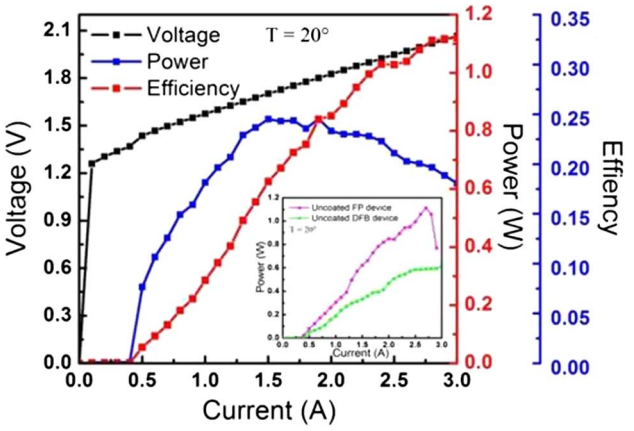

Fig. 6. PIV characteristics and electro-optical efficiency profiles of coated tapered DFB laser device. The inset shows the power–current characteristics comparison between uncoated tapered DFB and FP laser devices.

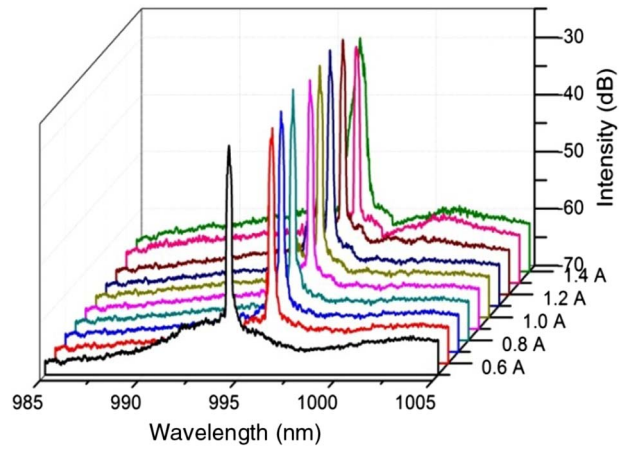

Fig. 7. Optical spectrum of the coated tapered gain-coupled DFB laser device from 0.5 A to 1.4 A.

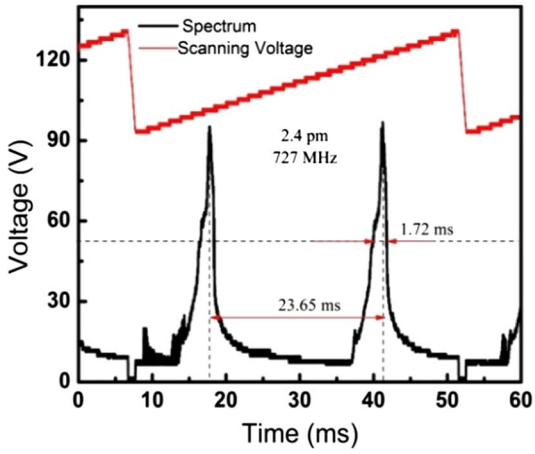

Fig. 8. Linewidth pattern of the coated tapered gain-coupled DFB laser device at 1.4 A.

CW operation are shown in Fig. 6. The inset shows the power–current (PI) characteristics comparison between the uncoated tapered DFB laser device and the FP laser device, only without surface-etched grooves. All of the devices were tested to 3 A. The optical output power of the coated tapered gain-coupled DFB laser device increases almost linearly without rollover or COD. Laser operation starts at 0.5 A. The output power of our device reaches up to 1.12 W at 3 A. and the maximum calculated electro-optical efficiency is more than 24.5% at an optical output power of 0.84 W. The slope efficiency is about 0.58 W/A, which is nearly 2 times as large as that of the uncoated device, and several times larger than 0.11 W/A of the reported gain-coupled DFB laser [35]. It has to be pointed out that, though the slope efficiency and the maximum output power of the DFB device are both inferior to the FP device, the PI curve of the DFB device is much smoother than the FP device's PI curve. This is because the DFB device works in SLM and FTM, and the shallow-etched grooves aside the ridge help filter out high-order modes and scatter the backreflection from the tapered waveguide. For comparison, the complex mode competition in the reference FP device causes the SHB and filament effect at high current, and the output power of the FP device sharply drops down at 2.7 A.

SLM operation is achieved from the threshold to 1.4 A, as the optical spectrum shows in Fig. 7. Our device keeps on-axis main-lobe emission up to 0.56 W and is an order of magnitude higher than our previously reported SLM lasers [17,30]. The maximum SMSR is over 38 dB at a current of 1.1 A at around 996 nm, which is higher than reported SLM lasers with surface index-coupled gratings [29]. The linewidth pattern measured at 1.4 A of the coated DFB laser device under CW operation is shown in Fig. 8. The 3 dB spectral linewidth of narrowband emission is only 2.4 pm at full width at half-maximum (FWHM), which is narrower than that of the 975 nm narrow-linewidth diode laser with the linewidth of 10 pm [12]. Our device works in MLM operation after 1.4 A. That is the main reason that causes the kinks of the PI curve of the tapered gain-coupled DFB laser device. The MLM operation occurs because the ridge DFB master oscillator reaches its gain saturation in large current injection, and there is no sufficient gain contrast to maintain SLM. This problem would be improved by the introduction of the separated electrodes, and the output power in SLM operation would be increased by proportionally lengthening the device in future work. The vertical and lateral far-field patterns of the tapered gain-coupled DFB laser device measured at 2.5 A are shown in Fig. 9. Far-field profiles are individually normalized at an intensity of 1. By implementing an asymmetric ULOC structure, the vertical far-field divergence angle at e^{-2} is drastically reduced to 28.02°. The lateral far-field divergence angle at e^{-2} is only 14.98°. The beam waist width is measured to be 7.96 μm after collimation, and the beam propagation ratio is $M^2 = 1.64$ ($1/e^2$ level), achieving an excellent near-diffraction-limit beam quality. All of the far-field patterns keep on-axis main-lobe near-Gaussian distribution over the entire tuning range, with minor changes in shape and width.

The tapered gain-coupled DFB laser device achieves high output power with excellent beam quality. The ULOC

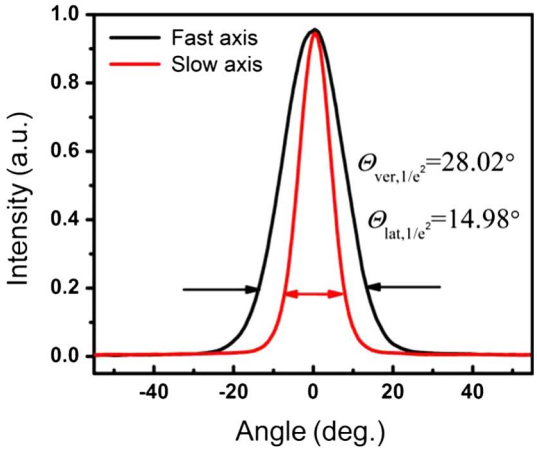

Fig. 9. Vertical and lateral far-field patterns of the coated tapered gain-coupled DFB laser device.

epitaxial layer structure improves the COD threshold and reduces the vertical far-field divergence angle. The narrow stripe ridge waveguide effectively restricts the optical field, obtains FTM operation, and narrows the lateral far field divergence angle. The periodic shallow-etched grooves provide SLM operation; the grooves aside the ridge waveguide provide scattering loss for high-order modes and scatter out backreflection from the tapered waveguide. The tapered waveguide enhances the output power and the COD threshold of the output facet, and the precise design of the parameters and the implementation of the gain-coupled mechanism weaken the far-field beam quality decrease effects such as the carrier- and temperature-induced refractive index perturbations occurring in the resonant cavity. Such stable characteristics weaken the trade-off between high output power and high beam quality of the ordinary semiconductor lasers.

4. CONCLUSION

In conclusion, a high-power, high-SMSR, narrow-linewidth, SLM, FTM, regrowth-free tapered gain-coupled DFB laser diode with periodic surface-etched grooves based on periodic current injection has been presented. The CW output power is up to 1.12 W at 3 A. The maximum slope efficiency is over 0.58 W/A, several times larger than the 0.11 W/A of the reported gain-coupled DFB laser [35]. The maximum electro-optical efficiency is over 24.5%. SLM emitting maintains from the threshold to 1.4 A. The maximum CW output power in SLM operation is more than 0.56 W, an order of magnitude higher than reported SLM lasers [17,30]. The 3 dB linewidth is less than 2.4 pm, narrower than that of 975 nm narrow-linewidth diode lasers [12]. The high SMSR of 38 dB at 996 nm is higher than lasers with surface index-coupled gratings [29]. The lateral far-field divergence angle is only 14.98°. The M^2 is 1.64, achieving a near-diffraction-limit beam quality. The device was fabricated with a simple micrometer-scale fabrication technique by standard i-line lithography. Based on the excellent electro-optical, spectral characteristics and simple technology, our device provides a practical low-cost method to realize high-power, high-SMSR, narrow-linewidth, SLM, FTM laser with high beam quality. Our device will be highly desirable for high-volume low-cost production in widespread commercial application areas.

Funding. National Science and Technology Major Project of China (2016YFE0126800); Frontier Science Key Program of the President of the Chinese Academy of Sciences (CAS) (QYZDY-SSW-JSC006); National Natural Science Foundation of China (NSFC) (11604328, 11874353, 51672264, 61474117, 61674148, 61727822, 61874119); Science and Technology Key Project of Jilin Province (20170204013GX); Open Fund of the State Key Laboratory of Integrated Optoelectronics (IOSKL2018KF21); Natural Science Foundation of Jilin Province (20160520017JH, 20170623024TC); Science and Technology Development Project of Jilin Province (20180201014GX).

REFERENCES

1. J. Fricke, W. John, A. Klehr, P. Ressel, L. Weixelbaum, H. Wenzel, and G. Erbert, "Properties and fabrication of high-order Bragg gratings for wavelength stabilization of diode lasers," Semicond. Sci. Technol. **27**, 055009 (2012).
2. K. Derikvand, Z. Chinipardaz, S. Ghasemi, and N. Chiniforush, "The versatility of 980 nm diode laser in dentistry: a case series," Journal of Lasers in Medicine **7**, 205–208 (2016).
3. L. Greusard and D. Costantini, "Near-field analysis of metallic DFB lasers at telecom wavelengths," Opt. Express **21**, 10422–10429 (2013).
4. G. P. Agrawal, *Fiber-Optic Communication Systems* (Wiley, 1997).
5. W. Schulz and R. Poprawe, "Manufacturing with novel high-power diode lasers," IEEE J. Sel. Top. Quantum Electron. **6**, 696–705 (2000).
6. J. J. Coleman, A. C. Bryce, and C. Jagadish, *Advances in Semiconductor Lasers* (Academic, 2012).
7. A. R. Nehrir, K. S. Repasky, and J. L. Carlsten, "Eye-safe diode-laser-based micropulse differential absorption lidar (DIAL) for water vapor profiling in the lower troposphere," J. Atmos. Ocean. Technol. **28**, 131–147 (2011).
8. B. W. Tilma, M. Mangold, C. A. Zaugg, S. M. Link, D. Waldburger, A. Klenner, A. S. Mayer, E. Gini, M. Golling, and U. Keller, "Recent advances in ultrafast semiconductor disk lasers," Light: Sci. Appl. **4**, e310 (2015).
9. E. C. Burrows and K. Y. Liou, "High resolution laser LIDAR utilising two-section distributed feedback semiconductor laser as a coherent source," Electron. Lett. **26**, 577–579 (1990).
10. Z. Zhou, B. Yin, and J. Michel, "On-chip light sources for silicon photonics," Light: Sci. Appl. **4**, e358 (2015).
11. S. Spiebberger, M. Schiemangk, A. Wicht, H. Wenzel, O. Brox, and G. Erbert, "Narrow linewidth DFB lasers emitting near a wavelength of 1064 nm," J. Lightwave Technol. **28**, 2611–2616 (2010).
12. T. N. Vu, A. Klehr, B. Sumpf, H. Wenzel, G. Erbert, and G. Trankle, "Tunable 975 nm nanosecond diode-laser-based master-oscillator power-amplifier system with 16.3 W peak power and narrow spectral linewidth below 10 pm," Opt. Lett. **39**, 5138–5141 (2014).
13. S. Tan, J. C. Zhang, and L. J. Wang, "Index-coupled multi-wavelength distributed feedback quantum cascade lasers based on sampled gratings," Opt. Quantum Electron. **46**, 1539–1546 (2014).
14. H. Kogelnik and C. V. Shank, "Coupled-wave theory of distributed feedback lasers," J. Appl. Phys. **43**, 2327–2335 (1972).
15. Y. Luo, Y. Nakano, K. Tada, T. Inoue, H. Hosomatsu, and H. Iwaoka, "Purely gain-coupled distributed feedback semiconductor laser," Appl. Phys. Lett. **56**, 1620–1622 (1990).
16. Y. Nakano, Y. Luo, and K. Tada, "Facet reflection independent, single longitudinal mode oscillation in a GaAlAs/GaAs distributed feedback laser equipped with a gain coupling mechanism," Appl. Phys. Lett. **55**, 1606–1608 (1989).
17. F. Gao, L. Qin, Y. Chen, P. Jia, C. Chen, L. Cheng, H. Chen, L. Liang, Y. Zeng, X. Zhang, H. Wu, Y. Ning, and L. Wang, "Study of

gain-coupled distributed feedback laser based on high order surface gain-coupled gratings," Opt. Commun. **410**, 936–940 (2018).
18. H. Soda, Y. Kotaki, H. Sudo, and H. Ishikawa, "Stability in single longitudinal mode operation in GaInAsP/InP phase adjusted DFB lasers," IEEE J. Quantum Electron. **23**, 804–814 (1987).
19. S. Nilsson, T. Kjellberg, T. Klinga, R. Schatz, J. Wallin, and K. Streubel, "Improved spectral characteristics of MQW-DFB lasers by incorporation of multiple phase-shifts," J. Lightwave Technol. **13**, 434–441 (1995).
20. J. Li, H. Wang, X. Chen, Z. Yin, Y. Shi, Y. Lu, Y. Dai, and H. Zhu, "Experimental demonstration of distributed feedback semiconductor lasers based on reconstruction equivalent-chirp technology," Opt. Express **17**, 5240–5245 (2009).
21. R. J. Guo, J. Lu, S. P. Liu, Y. C. Shi, Y. T. Zhou, Y. T. Chen, J. Luan, and X. F. Chen, "Multisection DFB tunable laser based on REC technique and tuning by injection current," IEEE Photon. J. **8**, 1–7 (2016).
22. S. Sujecki and L. Borruel, "Nonlinear properties of tapered laser cavities," IEEE J. Sel. Top. Quantum Electron. **9**, 823–834 (2003).
23. F. Gao, L. Qin, Y. Chen, P. Jia, C. Chen, L. Cheng, H. Chen, L. Liang, Y. Zeng, X. Zhang, Y. Ning, and L. Wang, "Narrow-strip single-longitudinal-mode laser based on periodic anodes defined by i-line lithography," IEEE Photon. J. **10**, 1–10 (2018).
24. F. J. Wilson, J. J. Lewandowski, B. K. Nayar, D. J. Robbins, P. J. Williams, N. Carr, and F. O. Robson, "9.5 W CW output power from high brightness 980 nm InGaAs/AlGaAs tapered laser arrays," Electron. Lett. **35**, 43–45 (1999).
25. A. Müller, J. Fricke, F. Bugge, O. Brox, G. Erbert, and B. Sumpf, "DBR tapered diode laser with 12.7 W output power and nearly diffraction-limited, narrowband emission at 1030 nm," Appl. Phys. B **122**, 87 (2016).
26. J. P. Donnelly, J. N. Walpole, S. H. Groves, R. J. Bailey, L. J. Missaggia, A. Napoleone, R. E. Reeder, and C. C. Cook, "1.5 μm tapered-gain-region lasers with high-CW output powers," IEEE Photon. Technol. Lett. **10**, 1377–1379 (1998).
27. H. Odriozola, J. M. G. Tijero, L. Borruel, and I. Esquivias, "Beam properties of 980-nm tapered lasers with separate contacts: experiments and simulations," IEEE J. Quantum Electron. **45**, 42–50 (2009).
28. Y. Shi, S. Li, R. Guo, R. Liu, Y. Zhou, and X. Chen, "A novel concavely apodized DFB semiconductor laser using common holographic exposure," Opt. Express **21**, 16022–16028 (2013).
29. L. Liu, H. Qu, Y. Wang, Y. Liu, Y. Zhang, and W. Zheng, "High-brightness single-mode double-tapered laser diodes with laterally coupled high-order surface grating," Opt. Lett. **39**, 3231–3234 (2014).
30. F. Gao, L. Qin, Y. Chen, P. Jia, C. Chen, H. Chen, L. Liang, Y. Zeng, X. Zhang, Y. Ning, Y. Zhang, and L. Wang, "Two-segment gain-coupled distributed feedback laser," IEEE Photon. J. **10**, 1500509 (2018).
31. Y. Chen, P. Jia, J. Zhang, L. Qin, H. Chen, F. Gao, X. Zhang, X. Shan, Y. Ning, and L. Wang, "Gain-coupled distributed feedback laser based on periodic surface anode canals," Appl. Opt. **54**, 8863–8866 (2015).
32. S. L. Chuang, *Physics of Photonic Devices* (Wiley, 2009).
33. M. Mikulla, "Tapered high-power, high-brightness diode lasers: design and performance," Top. Appl. Phys. **78**, 265–288 (2000).
34. S. F. Yu, "Double-tapered-waveguide distributed feedback lasers for high-power single-mode operation," IEEE J. Quantum Electron. **33**, 71–80 (1997).
35. T. W. Johannes, A. Rast, W. Harth, and J. Rieger, "Gain-coupled DFB lasers with a titanium surface Bragg grating," Electron. Lett. **31**, 370–371 (2002).